Technoeconomic Analysis and Design of CO_2 Capture and Conversion Systems

by

Simon B. Rufer

B.S. Mechanical Engineering
University of California Los Angeles, 2020

SUBMITTED TO THE DEPARTMENT OF MECHANICAL ENGINEERING IN PARTIAL FULFILLMENT OF THE REQUIREMENTS FOR THE DEGREE OF

MASTER OF SCIENCE IN MECHANICAL ENGINEERING
AT THE
MASSACHUSETTS INSTITUTE OF TECHNOLOGY

MAY 2022

Signature of Author: _____
Department of Mechanical Engineering
May 6, 2022

Certified by: _____
Kripa K. Varanasi
Professor of Mechanical Engineering
Thesis Supervisor

Accepted by: _____
Nicolas G. Hadjiconstantinou
Professor of Mechanical Engineering
Chairman, Committee of Graduate Studies

Technoeconomic Analysis and Design of CO_2 Capture and Conversion Systems

by

Simon B. Rufer

Submitted to the Department of Mechanical Engineering
on May 6, 2022 in Partial Fulfilment of the
Requirements for the Degree of Master of Science in
Mechanical Engineering

ABSTRACT

Carbon capture and conversion technologies must become economically viable and scale to the gigaton level by 2050 to avoid the most serious effects of a climate crisis. Here we present a techno-economic analysis of two promising capture and conversion technologies: CO_2 capture from ocean waters via electrochemical pH swing and electrochemical conversion of CO_2 into valuable chemicals. We identify cost drivers of the proposed direct ocean capture process and suggest future work to reduce costs and technological risks. Finally, we examine the sensitivities of the cost of CO_2 conversion with regards to the design of electrode gas diffusion layers. We design and construct a CO_2 conversion reactor for testing of next generation gas diffusion layers. Strong baseline performance of the reactor is validated with a 47% Faradaic Efficiency towards C_2H_4 at 200mA/cm^2.

Thesis Supervisor: Kripa K. Varanasi
Title: Professor of Mechanical Engineering

Acknowledgements

Despite the start of my program coinciding with a global pandemic and lockdowns, Kripa Varanasi enthusiastically and optimistically welcomed me into the MIT community as my advisor and mentor. I am incredibly thankful to have received his thoughtful support and his sharp technical guidance over the last two years: his mentorship has been central to my personal development. I am eager to continue working together to build something great.

The members of the Varanasi Lab group have shown me what collaboration can be at its finest. I deeply respect each and every one of you, and I am thankful for the intellectual depth which our conversations have added to my journey at MIT. Just as importantly, the friendly lab space and lively attitude has always served as a welcomed source of relaxation and happiness. For these reasons, I thank Bert, Vishnu, Sreedath, Jack, Mike, Baptiste, Tal, Caroline, Sean, Fabian, and Victor.

I could not call Boston a home without my friends, who are so talented at turning any regular day into a delightful and exciting journey. To all my friends across the coasts and overseas, I look forward to the days we reconnect. Thank you to all of you for your support and care, I could not have done this without you.

Finally, a big thank you goes out to my family for 23 years of unwavering support and for preparing me to make the most of every opportunity I've been blessed with.

Table of Contents

List of Figures

1 Introduction

To avoid the most dire societal effects of climate change, the 2015 Paris Climate Agreement outlines the reduction of Carbon Dioxide (CO_2) and other Green House Gas (GHG) emissions to net-zero by mid-century[1]. Broad-reaching action must be taken to meet this goal, including shifting consumer habits, improving efficiencies, increasing renewable energy penetration, developing carbon-free alternative technologies, and carbon capture and sequestration[2]. There are no silver bullet technologies for this challenge, because the technological and economic constraints of each GHG-emitting industry are unique – innovation is necessary on all fronts. In 2020, about 20% of the 33Gt global CO_2 emissions originated from difficult to decarbonize industries. These industries, including cement, aviation, and metal production serve critical functions to society but face significant intrinsic barriers to complete decarbonization. Carbon capture and conversion must therefore be a significant focus of technology development in the net-zero case. The International Energy Agency (IEA) calls for 7.6 Gt/yr carbon capture capacity by the year 2050[2].

Carbon capture solutions can take many forms. Point Source CO_2 enables potential net-zero emissions of otherwise-emitting processes by stripping CO_2 from their waste streams. Carbon capture can also be achieved from more dilute, environmental sources like the air, the oceans, or biomass. Subsequent long-term sequestration of CO_2 capture from environmental sources presents an opportunity for net-negative CO_2 emissions. The IEA projects a need for 1.0Gt CO_2 per year of net-negative capacity by 2050[2]. Though technologies such as Direct Air Capture (DAC) which capture CO_2 directly from the atmosphere have received significant attention and investment, their costs remain high. Climeworks, a leading DAC company, currently prices CO_2 emissions at $600/tonne[3], while Carbon Engineering's highly optimistic estimates lie between $94-$232/tonne[4]. These numbers fall short of the US Department of Energy (DOE) target of <$100/tonne CO_2[5] and motivates the continued exploration and development of novel technologies which can reduce costs and accelerate adoption.

The development of technologies which transform captured CO_2 into profitable products has been suggested as a means to reduce the effective cost of capturing CO_2. Moreover, the

conversion of CO_2 into useful products could also serve to sequester CO_2 emissions, establishing these upscaling technologies as net-negative. The use of CO_2 as an asset rather than a waste could pave the way to a sustainable and circular carbon economy.

In this thesis, I will investigate technologies which address both Carbon Capture and CO_2 Conversion with a focus on reducing cost and enabling scalability. In the first part of the thesis, I explore a novel Direct Ocean Capture (DOC) Carbon removal process through the lens of a techno-economic analysis. In the second part of the thesis, I briefly outline the economics of electrochemical CO_2 conversion before delving into the design and testing of a CO_2 conversion reactor useful for the development of commercially viable electrodes.

2 Direct Ocean Capture

2.1 Motivation

The IEA pathway projects the use of DAC and Bio Energy with Carbon Capture and Storage (BECCS) will meet global CO_2 removal needs of 1.0Gt/yr by 2050. However, CO_2 removal rates of these early-stage technologies was only 40Mt/yr in 2020, reflecting the great need to develop carbon-negative technologies which can scale quickly and economically[2]. Direct Ocean Capture (DOC) of CO_2 has been proposed as an alternative approach for carbon-negative removal. Increases in atmospheric CO_2 concentrations from anthropogenic emissions have led to a corresponding increase in CO_2 content within the ocean waters themselves. In fact, about 40% of emissions since the beginning of the industrial revolution have been absorbed by the oceans[6,7]. As the atmosphere and oceans equilibrate, removal of CO_2 from the oceans results in a corresponding decrease in atmospheric CO_2 concentrations. CO_2 dissolves in oceanwater and subsequently forms a buffer system with bicarbonate and carbonate:

$$HCO_3^- + H^+ \leftrightarrow H_2CO_3 \leftrightarrow CO_2 + H_2O \quad (1)$$

The CO_2 content of the oceans is thus best described by the amount of Dissolved Inorganic Carbon (DIC) which includes CO_2, CO_3^{2-}, and HCO_3^-. DIC concentrations in oceanwater are relatively high on a volumetric basis at approximately 100mg/L[8]. Notably, the concentration of CO_2 in air is only 0.77mg/L (~400 ppm), indicating that DOC approaches may have less constraining fluid handling requirements than DAC. Moreover, leading DAC technologies use absorption or adsorption techniques which require the CO_2 to first be absorbed or adsorbed and then released from the sorbent/adsorbent. DOC provides a possible simplification of this process, as CO_2 is already dissolved within ocean water, requiring only the release step before CO_2 is obtained. Given the potential benefits of DOC and the global need for a number of diverse carbon mitigation strategies, DOC is a promising approach for carbon capture in addition to the more well-established DAC and BECCS.

2.2 Current Approaches and Limitations

The bicarbonate – carbonate – carbon dioxide buffer system in Equation (1) can be shifted by adding or removing H+ ions, that is, via pH modulation. When oceanwater is sufficiently acidified to a pH of approximately 6, the majority of the DIC in the water becomes CO_2 and can be released in the gas phase. When alkalized, the equilibrium shifts in the other direction, producing carbonate precipitates. This mechanism was employed by Eisaman et al. in their bipolar membrane electrodialysis (BPMED) process which produced separate acidified and alkalized process streams from which CO_2 could be captured and mineralized[9–11]. An energy consumption of 242kJ/mol CO_2 was achieved for 59% CO_2 extraction efficiency[9]. The energy intensity of BPMED processes was reduced to 155kJ/mol CO_2 by Digdaya et al. through use of a redox couple in the electrolyte[12]. Though BPMED processes show promise with relatively low energetics, the use of membranes could incur significant cost penalties. The use of toxic redox couples also poses concerns over leakage and potential damage to marine wildlife. Electro-deionization systems have also been developed, which split water to evolve Hydrogen and Oxygen as useful byproducts while acidifying a central oceanwater stream bounded on either side by cation exchange membranes for CO_2 release[13]. This approach involves the use of expensive membranes and has poor energetics per mol of CO_2 released due to the large minimum thermodynamic potential required to split water. It also requires the addition of significant quantities of de-ionized water.

A scalable solution is sought which achieves excellent energy- and CO_2 extraction-efficiencies without the need for additives or expensive membranes.

2.3 DOC Cell Design

Prior work by the Hatton group at MIT has identified a promising chemical-free, low-energy, and membrane-less approach for electrochemical pH-swing release of CO_2 from ocean water. The oxidation of bismuth is used to release protons into the solution:

$$Bi + Cl^- + H_2O \leftrightarrow BiOCl + 2H^+ + 3e^- \qquad E^o = 0.16V \text{ (vs SHE)} \qquad (2)$$

To enable a pH swing in a membrane-less configuration, the second half reaction is chosen to be a Chloride ion release from an AgCl electrode:

$$AgCl + e^- \leftrightarrow Ag^+ + Cl^- \qquad E^o = 0.23V \text{ (vs SHE)} \qquad (3)$$

The Ag and Bi catalyst form the two electrodes of an asymmetric cell capable of swinging the electrolyte pH and is shown in Figure 1. Because the reaction chemically alters the electrodes, the cells have a finite proton release or proton absorption capacity related to the quantity and surface availability of active material. A cycle analogous to battery charging and discharging can be envisioned where an individual cell first acts to acidify the ocean water stream by proton release until its capacity is reached. When the polarity on the cell is switched, the capacity of the electrodes is regenerated while the feed stream is alkalized. By using two such cells, oceanwater can be acidified by a first cell allowing for gas-phase CO_2 removal. A second cell then re-alkalizes the oceanwater stream such that it can safely be discharged back into the ocean. The process is shown below in Figure 1. Due to the charging and discharging nature of the electrodes, the feed stream of each individual cell must be periodically switched between fresh oceanwater and acidified oceanwater.

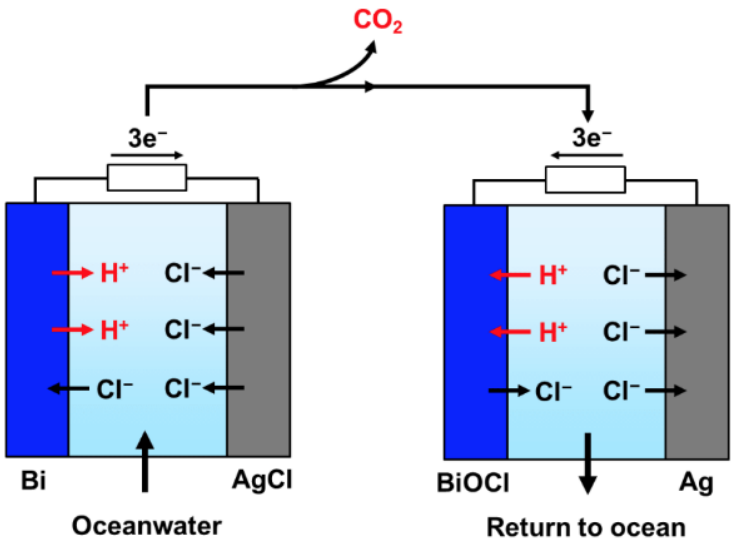

Figure 1: A cycle using asymmetric Bi and AgCl electrodes for removal of CO_2 from oceanwater. The first cell acidifies the oceanwater and the second cell re-alkalizes the oceanwater before discharge.

This proposed cycle does not use chemical additives, expensive membranes, and has a very low theoretical energy requirement. Preliminary unpublished experimental results show an experimental energy use of 122kJ/mol of CO_2.

2.4 DOC System Design

A system employing the asymmetric pH-swing cells for large-scale CO_2 capture was conceptually designed to estimate its cost per tonne of CO_2 captured.

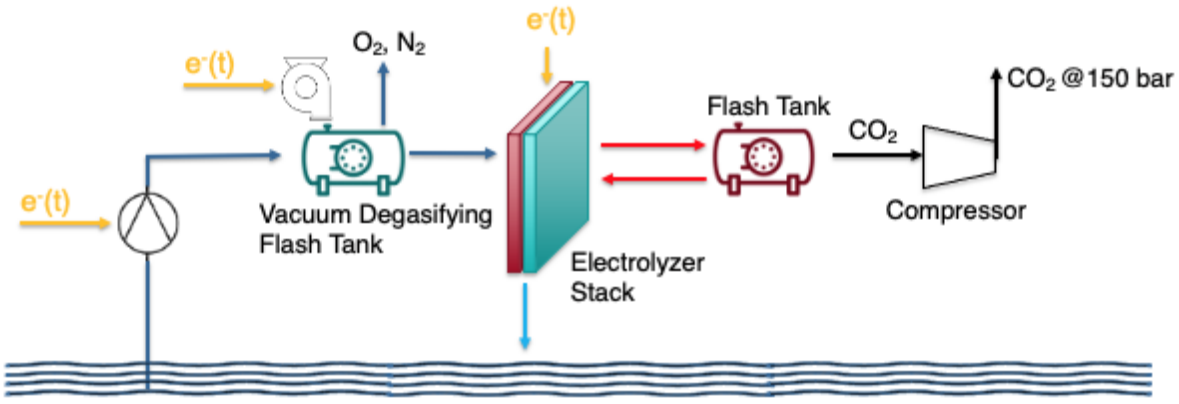

Figure 2: System for separation of CO_2 from oceanwater using electrolyzer stacks composed of asymmetric pH swing cells. Oceanwater is pumped from the ocean into a primary vacuum degasifying flash tank, where O_2 and N_2 are removed. The electrolyzer stack acidifies the DIC-rich stream via proton release, and the CO_2 is separated in a subsequent flash tank. The acidified CO_2-lean stream is then alkalized with the reverse reaction in the electrolyzer stack and discharged back to the ocean at the appropriate pH. The CO_2 is then compressed to 150bar.

Because the partial pressure of CO_2 in oceanwater is only 0.07atm upon acidification, a vacuum must be pulled on the oceanwater below this pressure to remove the CO_2 in a gaseous phase. Dissolved Oxygen gas (8mg/L of oceanwater) and Nitrogen gas (16mg/L of oceanwater) will also be released under these vacuum conditions[14]. Though the concentration of DIC exceeds the concentration of O_2 and N_2, simultaneous removal would result in a process stream of, at best, ~80% CO_2. To ensure a higher purity CO_2 stream for compression and transport, a vacuum degassing flash tank *precedes* the electrolyzer stack to remove a majority of the Oxygen and Nitrogen before acidification and CO_2 release. At this stage, the majority of CO_2 is in carbonate of bicarbonate form rather than dissolved CO_2, avoiding premature CO_2 loss. The oceanwater stream stripped of Oxygen and Nitrogen is fed into the Electrolyzer stack composed of the asymmetric Bismuth/Ag/AgCl cells. The acidified oceanwater is then fed into a second flash tank, which facilitates the thermodynamically favorable release of CO_2. The flash tank serves to increase the interfacial surface area of interaction between the vacuum environment and the

acidified CO_2-rich oceanwater such that the reaction proceeds quickly and completely. Following the second flash tank, the CO_2 is compressed to 150 bar for transport.

For the purposes of this model, our plant is assumed to have a production capacity of 1MT CO_2 per year for a 20 year lifetime. A capital recovery factor (CRF) of 10% is used. All electricity is assumed to come from renewable sources and therefore carries no carbon footprint. An electricity cost of $0.02/kWh is used in light of recent PV PPA prices which have already begun to dip below $0.03/kWh[15] and are expected to approach $0.02/kWh in the future. A capacity factor of 0.4 is used to account for the intermittency of these low-cost renewable sources[16]. Throughout this analysis, we compare sub-system costs to a total cost allowance of $100/tonne CO_2, which is the ultimate project goal aligning with the DOE EarthShot[5].

This techno-economic analysis considers only the cost of the systems specific to the CO_2 separation process detailed above. Costs associated with the intake and pre-processing of oceanwater are outside of the scope of this analysis, though these costs are known to be quite significant[10,12]. As explored below, the proposed process has a low pressure drop across the electrolyzer stack, which may help to reduce this cost component in future analyses. Costs associated with the land or facilities (i.e. floating platform or oil rig for off-shore implementations) required are also neglected. These assumptions are most realistic for co-location with a desalination plant which already processes and pumps significant amounts of water.

2.5 Electrolyzer Stack Capital Costs

Cost estimates for our electrolyzer stack are estimated using the known cost of existing alkaline electrolyzer technology. Alkaline electrolyzers are used as a proxy because they are relatively mature and well-understood, and the fluid handling infrastructure, materials of construction, and pH conditions are similar to the conditions in our proposed cell. The 1MT CO_2/year capacity of the plant combined with the projected 2.0GJ/t CO_2 electrochemical energy requirement determined by Hatton et al. and the 0.4 capacity factor yield an operational plant power of 158MW. Note that the capacity factor plays a significant role here in increasing the required plant power by a factor of 2.5x compared to full duty-cycle operation, and exposes an

interesting optimization problem. A second plant design could be considered which leverages a higher capacity factor available for higher-cost or higher carbon-intensity electricity. Such a plant would feature substantially decreased electrolyzer stack CAPEX, though at the expense of higher electricity operating costs as well as decreased net carbon capture efficiency. This optimization is not further explored herein but would nonetheless be a valuable analysis. The estimated investment cost for alkaline electrolyzers per kW at the ~100MW scale is $370/kW[17] and is shown in Figure 3a.

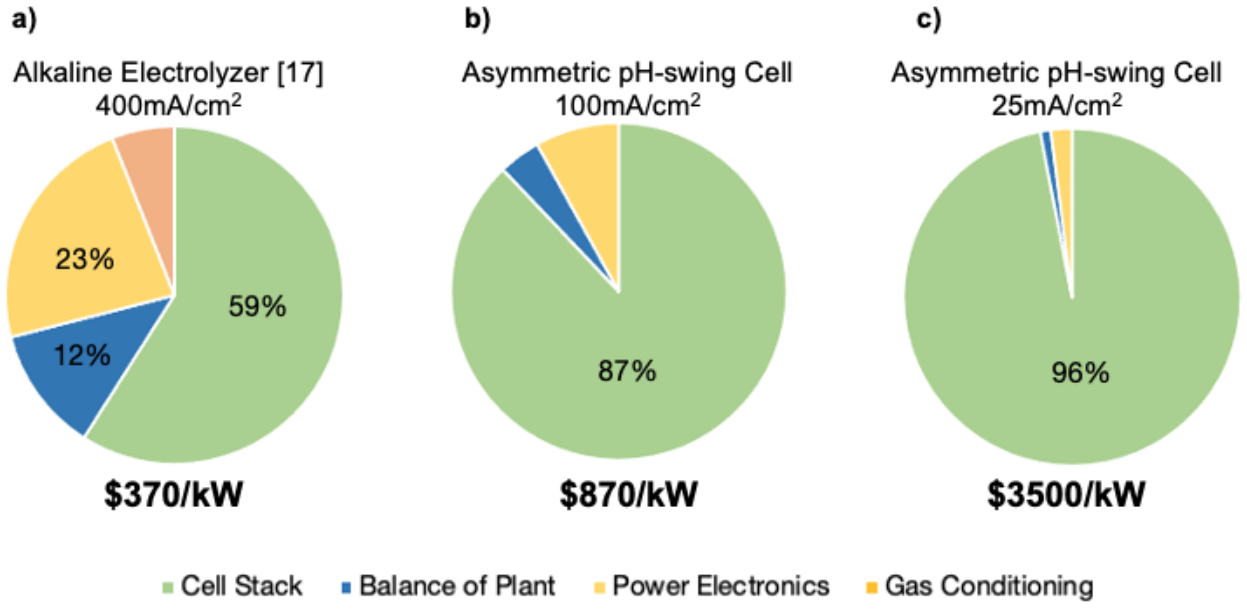

Figure 3: a) Total investment cost of alkaline electrolyzer stacks, broken down by cost components. Data is reproduced from [17] with a reference current density of 400mA/cm^2. b) Adjusted cost fractions used for the following analysis for an asymmetric pH-swing cell with a current density of 100mA/cm^2. c) Adjusted cost fractions used for the following analysis for an asymmetric pH-swing cell with a current density of 25mA/cm^2. Note that gas processing costs are neglected in b) and c) because these costs are considered in the gas processing subsystem.

The specification of electrolyzer CAPEX in units of $/kW relies on the assumption of a reference current density, as the CAPEX of materials is more closely related to the actual physical size of the electrolyzer stack rather than its power. Because the electrolyzer stacks used in our system are expected to operate at a different current density than the one used in [17], we scale the cell stack CAPEX cost component by the relative current densities. For the purposes of

this analysis, we assume two cases of 25mA/cm^2 and 100mA/cm^2 which are shown in Figure 3b) and 3c). Electrolyzers with a lower current density should have higher costs per kW, and a linear assumption leads us to stack costs for 25mA/cm^2 and 100mA/cm^2 current densities which are 16 and 4 times higher, respectively, than those for a 400mA/cm^2 electrolyzer in Figure 3a). Power electronics and balance of plant (BOP) are not scaled according to current density, as these costs are expected to scale with total stack power rather than geometric area. Bismuth and Ag catalyst costs are excluded from this analysis. The reference cost per kW of electrolyzer stack already considers the catalyst cost, which amounts to less than 4% of the total cost for the reference alkalize electrolyzers using nickel catalysts. By keen design and catalyst loading optimization, these costs are expected to be kept low even when considering precious metals: PEM electrolyzers using expensive Platinum and Iridium catalysts still maintain catalyst costs at only 4% of their total electrolyzer stack cost[17].

The preceding assumptions yield investment cost estimates of $870/kW in the 100mA/cm^2 case and $3500/kW in the 25mA/cm^2 case. When levelized over a 20 year period, the electrolyzer stack costs incur a $16/t CO2 and $65/t CO_2 cost for the high and low current density case. Pushing the maximum achievable current density of these cells beyond 10's of mA/cm^2 and to the 100mA/cm^2 level should therefore be a critical focus of development efforts, as Electrolyzer Stack costs otherwise assume the bulk of the $100/t CO_2 cost allowance.

Further investigation and system design may reduce electrolyzer CAPEX costs as the specific functional requirements of our process are considered beyond those in the alkaline electrolyzer cost reference. Future analyses should consider the feasibility of lower-cost materials such as plastics and whether novel system architectures may help to reduce this estimate.

2.6 Electrolyzer Stack Operating Costs

With an assumed electricity cost of $0.02/kWh and a process energy requirement of 2.0GJ/t CO_2, electricity costs are readily calculated at $11/t CO_2. This low energy cost accounts for just 11% of the cost allowance and is to be expected by the favorable energetics of the electrochemical pH swing process.

2.7 Pumping Costs

To reach 1Mt CO_2 /year with a capacity factor of 0.4 and a capture efficiency of 85%, the plant must process 940m^3/s of oceanwater given DIC of 2.3mM in oceanwater. The system pressure drop should be minimized in consideration of this rather large flowrate to avoid large pumping penalties. For this analysis, we assume that the bulk fluid handling system is well designed with large diameter piping and with minimal required elevation head such that the dominant pressure drop in the system is that through the millimetric flow gap of the electrochemical cell. Our modular cells are assumed to be square in shape, with 1m^2 area and a 2.5mm inter-electrode gap as has been used throughout modelling efforts. The flowrate of oceanwater through the cells can be calculated by matching the proton flux at a given geometric current density of the electrode to the flux of DIC in the oceanwater while accounting for the 3/2 ratio of electrons to protons released as shown in equation (2). At current densities below 50mA/cm^2, the flow remains laminar with a Re of less than 5x10^5, and thus the Hagen-Poiseulle equation can be used to calculate an approximate pressure drop associated with the flow through the cells:

$$\Delta P = \frac{12\mu L Q}{h^3} \tag{4}$$

Where μ is the viscosity of oceanwater (1.17cP), L is the cell length (1m), Q is the flowrate per cell, and h is the inter-electrode gap of 2.5mm. The fluid streams must pass through two sequential acidifying and basifying cells, so the pressure drop is multiplied by 2. Finally, a conservative factor of safety of 2 is added to account for losses in other tubing as well as a possible transition to turbulence for cells with higher current densities. The resultant total pumping power is 2.6MW and 10.4MW for 25mA/cm^2 and 100mA/cm^2, respectively. With a conservative pump efficiency of 0.4, electricity costs for pump power total to \$0.45/tCO_2 and \$1.81/tCO_2 for the two current densities. CAPEX is estimated using industrial guidelines for pump costs in \$/kW[18], and when levelized, total to less than \$1/t CO_2.

Though pumping costs are on the order of single \$ per tonne of CO_2, a sensitivity analysis reveals that these costs could increase significantly outside of the current design choices. Pumping costs scale with electrode area to the $\frac{3}{2}$ power, electrode gap to the -3 power, and

linearly with current density. Moving forward, the electrochemical cell geometry should be carefully designed with these constraints in mind.

Moreover, pumping CAPEX is calculated under the assumption that the pumps used in the system are similar to typical industrial pumps[18]. However, the extraordinarily large volumes of water pumped in our application has the potential to provide some unique challenges. It is possible that our system design can be quite modular and use a large number of standard pumps in parallel. However, if this degree of modularity is difficult to achieve then large, specialized pumps could be required. Such specialized high-flow rate and low-pressure-drop pumps could significantly increase pumping costs. The modularity and overall size of this system should be carefully considered moving forward.

2.8 Gas Processing Costs

The gas processing system consists of the CO_2 compressor, vacuum pumps required for vacuum degasification, and the two flash tank vessels required for pre-extraction of O_2 and N_2 and the extraction of CO_2. The levelized cost of CO_2 compression to 150 bar is assumed to be \$15/t CO_2 based on several recent estimates ranging from \$12-\$22[19–21].

To compute the energy costs associated with the vacuum degasification, the following equation is used which approximates the power P of adiabatic compression:

$$P = \frac{kWRT}{k-1}\left(\left(\frac{p_{out}}{p_{in}}\right)^{\frac{k-1}{k}} - 1\right) \tag{5}$$

Where k is the heat capacity ratio of the gas, W is the combined molar flowrate of the gasses, R is the gas constant, T is the inlet temperature, and p_{out} and p_{in} are the absolute discharge and inlet pressures[22]. The dominating molar flux is expected to be vaporized water. Water vapor has a partial pressure under these conditions of 0.03atm, meaning vacuum pressures below this value would result in the complete vaporization of the water. A vacuum pressure of 0.04 atm is chosen to remove as much O_2 and N_2 as possible while avoiding steep penalties of

excessive water vaporization. To estimate the molar gas fluxes in equation (5), it is assumed that the entirety of the 8mg/L of O_2 and 16 mg/L of N_2 is removed from the oceanwater which is processed at the processing rate of 940m^3/s. To estimate the molar gas flux of water vapor, a first order approximation is made using the relative partial pressures of water vapor and O_2 and N_2 gasses. The difference in vacuum pressure (0.04 atm) and water vapor pressure (0.03atm) of 0.01 atm is assumed to be the partial pressure of O_2 and N_2 in the discharged gas stream under vacuum. The partial mol fluxes of water (W_{H_2O}), O_2, (W_{O_2}) and N_2 (W_{N_2}) are assumed to be linearly related to their partial pressures as shown below:

$$\frac{W_{H_2O}}{W_{O_2} + W_{N_2}} = \frac{p_{H_2O}}{p_{O_2} + p_{N_2}} = 3 \tag{6}$$

Thus we estimate the water flux as 3 times that of the combined O_2 and N_2 molar fluxes. This first-order estimation procedure holds in the limit, as pulling a vacuum at the partial pressure of water vapor would result in the complete vaporization of the water and an infinite ratio between the two. In using the adiabatic compression equation with the appropriate constants, we find that the vacuum power required is nearly 40MW, approximately 1/4th of the electrochemical power. This results in a total operating cost addition of $3/tCO2.

The structure and CAPEX of the flash tank process vessels within which the two vacuum degassing stages occurs is highly dependent on the ease with which the O_2, N_2, and CO_2 gasses evolve from their dissolved state within oceanwater. These reaction characteristics have not yet been thoroughly investigated, and as such we do not have strong estimates for the associated CAPEX. On one extreme, if the process happens instantaneously fast, then a simple bulk holding vessel would be required and a low levelized CAPEX on the order of single $ per tonne CO_2 would be expected. However, if the gas evolution reaction is significantly limited by kinetics or mass transport, a more complicated process vessel which increases the interfacial interaction area such as a packed bed would be required. This would greatly increase capital costs and operational costs due to added pressure drops and increased infrastructure, though the degree by which has not yet been determined.

In order to make some estimate of the required capital cost of the flash tank process vessels, the gas evolution reactions are assumed to require a residence of 10 seconds to fully complete. This assumption is exceedingly rough, but will serve to give some intuition for the estimated costs of these process vessels that can later be revisited. Given the 940m^3/s flowrate of oceanwater, 9,400m^3/s of vacuum capacity is required. This capacity is met with a design of 12 horizontal stainless-steel-clad vacuum process vessels with 10 meter diameter and 10 meter length. These dimensions are sized to fit within maximum cost estimation bounds of [18]. The capital required for construction and installation (Lang Factor = 4.74) of these vessels is found to be quite significant, with levelized costs coming to \$29/t CO_2.

2.9 Summary and Discussion

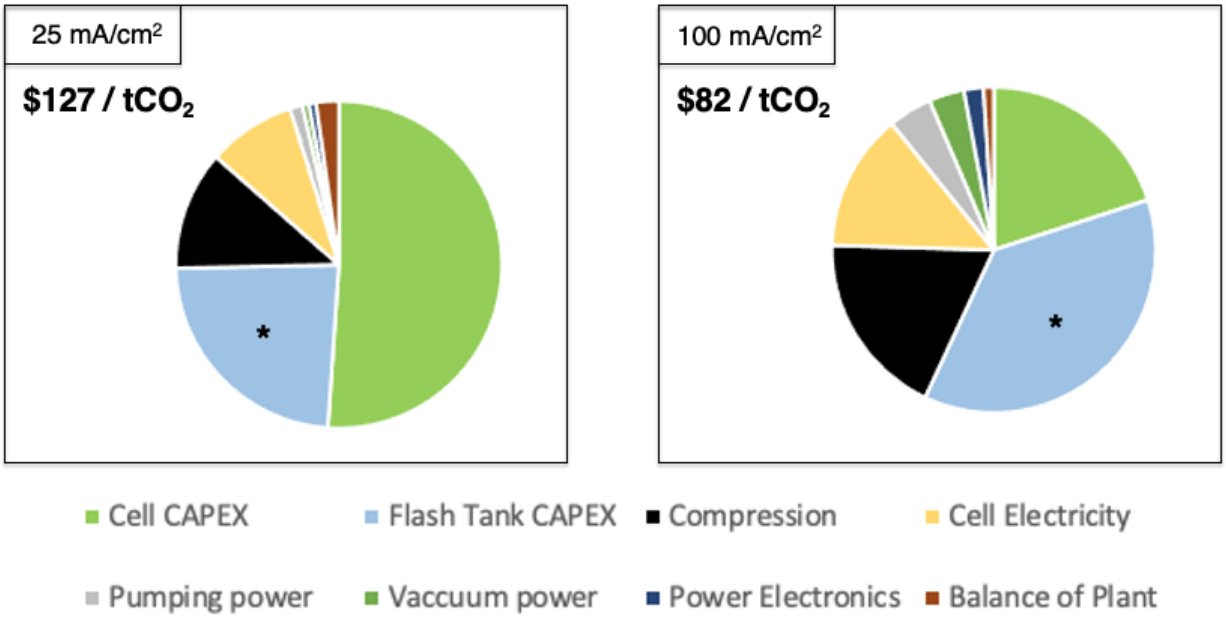

Figure 4: Total levelized cost per tonne of CO_2 captured at the two reference current densities.

Taken together, this technoeconomic model suggests that costs of under \$100/t CO_2 are possible with the novel electrochemical asymmetric pH-swing process. At lower current densities, the cell CAPEX (Electrolyzer Stack costs) dominate due to large required areas. At high current densities, this cost component is reduced, while compression, electricity, and flash tank CAPEX costs become more relevant.

The technoeconomic model also serves to identify areas in which additional research and technological advancement is necessary to de-risk the technology and further reduce costs. One such area is the maximum achievable current density of the electrodes. For economic feasibility, stable operation at least 25mA/cm^2 is imperative, though assumptions for electrolyzer cost per kW should be revisited. A geographic study and electricity capacity factor study could prove valuable by shedding light on the optimization between operational electricity costs and CAPEX costs associated with large electrolyzer stacks. Given the massive flowrates required for a large 1MT/year plant, future investigation should consider the modularity and specific module size of such a plant, particularly with respect to cost optimization with pump sizing. Moreover, additional investigation is required to determine the mass transport or kinetic limitations for the

process of O_2, N_2, and CO_2 gaseous evolution from oceanwater. If this process is exceedingly bottlenecked by mass transport or is otherwise a slow reaction, extensive infrastructure and correspondingly high CAPEX costs could follow. Future technoeconomic models may also begin to consider the auxiliary oceanwater intake costs which a stand-alone plant would face, and in particular, how the specifics of this pH-swing process and cell design interplay with intake costs.

3 CO_2 Conversion

3.1 Motivation

CO_2 has historically been discarded as a waste stream. Development of technologies which can alternatively use CO_2 as a reactant for producing valuable products would help to incentivize carbon capture by reducing its effective cost. Moreover, CO_2 conversion products hold the exciting possibility of displacing products conventionally produced as derivatives of fossil fuels. These conventional processes are themselves highly polluting: the production of petrochemicals accounts for 18% of industrial CO2 emissions at 1.5 Gt CO_2/yr[23]. The development of low-carbon intensity CO_2 conversion technologies at scale therefore stands to create a more sustainable carbon economy independent of finite fossil fuel resources. CO_2 conversion can also be a carbon-negative technology if the products are stable (such as plastics) and are not combusted or degraded.

A number of CO_2 conversion approaches have been suggested[24]. High-temperature thermochemical means for conversion of CO_2 into chemicals using co-reactants such as Hydrogen and Methane is possible using Nickel catalysts. However, the high temperature requirement (900ºC) and necessity of co-reactants complexifies the process. Moreover, it is limited to production of gaseous products[25]. Photochemical and photothermal methods have also been proposed but typically suffer from low energy efficiency and a limited range of products[24]. Though it is not expressly conversion, biocatalytic production of hydrocarbons fulfils the same objective of displacing conventional fossil-fuel based production methods. Biocatalytic processes utilize engineered enzymes to convert precursor molecules into valuable products such as ethylene and ethanol[26–28]. Though this approach is cost-competitive in some locales with the proper resource availability[26], its costs remain higher than those of fossil fuel alternatives. While biocatalytic production does show a reduction in CO_2 emissions compared to conventional methods, it remains a carbon-positive process owing to intensive farmland use. Finally, amendment of existing conventional processes via electrification of heating[29] and implementation of carbon capture infrastructure has been suggested to reduce carbon impact of these existing processes. While net-zero carbon emissions may be secured by these means, high-temperature electrical heating approaches are complex given the intermittent nature of renewable electricity, and these suggestions sustain societal reliance on limited reserves of fossil fuels.

CO_2 Conversion via electrochemical means (CO_2R), on the other hand, holds promise for scalability due to its low-temperature operation and its ability to produce a broad variety of products including complex multi-carbon products using only CO_2, water, and electricity. As with other electrolyzer technologies, it can ramp production easily on and off, making it amenable to intermittent renewable energy sources, and when operated on low-carbon-intensity electricity it can be carbon-negative[30]. Electrochemical CO_2 conversion was first explored in the pioneering work of Hori et al. in the 1980's,[31–33] and the field has enjoyed rapidly increasing interest in the last decade. In 2012, Kuhl et al. showed that 16 distinct products with as many as 3 Carbon atoms could be formed via the electroreduction of CO_2 at a metallic copper cathode[34]. Among these products, those attracting the greatest commercial interest are Ethylene (C_2H_4) and Ethanol (C_2H_5OH) owing to their large market size, significant possible emissions reductions, and moderate value density. The global production of Ethylene and Ethanol hold market sizes of $230B and $75B respectively, and complete electrochemical production of these products would result in reductions of global CO_2 emissions of 862MT CO_2 and 546Mt CO_2 respectively[30]. The price point of these C_2 produced electrochemically may become competitive with conventional methods owing to their high product value per tonne[35,36]. However, current ethylene and ethanol production via electrochemical means remains significantly more expensive than conventional means[30,35,36], motivating the pursuit of cost-effective developments for this technology.

3.2 Electrochemical CO_2R Background

The cathodic half-cell reactions for the electrochemical production of Ethylene and Ethanol are shown below under basic conditions:

$$2CO_2 + 8H_2O + 12e^- \rightarrow C_2H_4 + 12OH^- \quad (7)$$

$$2CO_2 + 9H_2O + 12e^- \rightarrow C_2H_5OH + 12OH^- \quad (8)$$

The corresponding anodic half reaction is typically Oxygen evolution, though oxidation of glycerol has been suggested to reduce energy usage[37]. The cathodic reaction must take place at the interface between an aqueous electrolyte which supplies the water and a solid conductive catalyst which supplies the electrons and catalytic sites. The CO_2 must therefore be in an aqueous phase for the reaction to proceed. The required dissolution of CO_2 in an aqueous phase imposes a unique challenge which plays a key role in the design of efficient CO_2 reduction (CO_2R) systems. Specifically, CO_2 has poor mass transport characteristics in aqueous solutions owing to

its low solubility and low diffusion constant, which severely limit the possible reaction rates and thus current densities of the reaction[38]. This is particularly true in alkaline pHs which are used to suppress HER, where CO_2 quickly reacts with OH^- to form a carbonate, reducing the penetration depth of CO2 to less than 1um into the solution[39]. This mass transport bottleneck poses limitations to the maximum achievable current density, and designs which alleviate this bottleneck will be explored in subsequent sections. First, a techno-economic analysis is performed to elucidate the importance of the current density for commercial viability.

3.3 Techno-Economic Analysis: Current Density as a Cost Driver

The current density achievable by a CO_2R system, expressed in milliamperes per square centimeter, determines the physical size of the electrolyzer stack for a given production rate. The electrolyzer stack CAPEX can be estimated by adopting a cost per unit area of electrolyzer from more mature existing electrolyzer technologies such as alkaline electrolyzers. The design requirements and construction of these electrolyzer stacks is similar to those of eventual CO_2R reactors with regards to electrolyte pH, power requirements, and pumping systems, making this comparison acceptable. In these systems, the cost of the catalyst and electrode are typically only a small fraction of the cost at less than 5% of the total cost[17], so differences in catalysts and electrode configurations are neglected. For this first-order analysis, the dominant cost sensitivity for the electrolyzer stack CAPEX is assumed to be the variation of the current density, which changes the required stack size. It is also assumed that improvements in current density are achieved at a constant cell voltage through technological development.

Under these assumptions, an existing technoeconomic framework by Sisler et al.[36] was modified to demonstrate the effect of current density on the CAPEX and therefore the total cost of ethylene production. Shown in Figure 5, the total cost estimate of ethylene production is compared to a price target of $1000/tonne of ethylene, an approximate cost of producing ethylene via conventional fossil fuel means. Critical technoeconomic model parameters include electricity at $0.02/kWh, a capital recovery factor (CRF) of 7%, a stack lifetime of 20 years, catalyst/electrode lifetime of 5 years, Faradaic Efficiency (FE) of 90%, stack voltage of 2.0V, and a CO_2 input cost of $30/tonne[36].

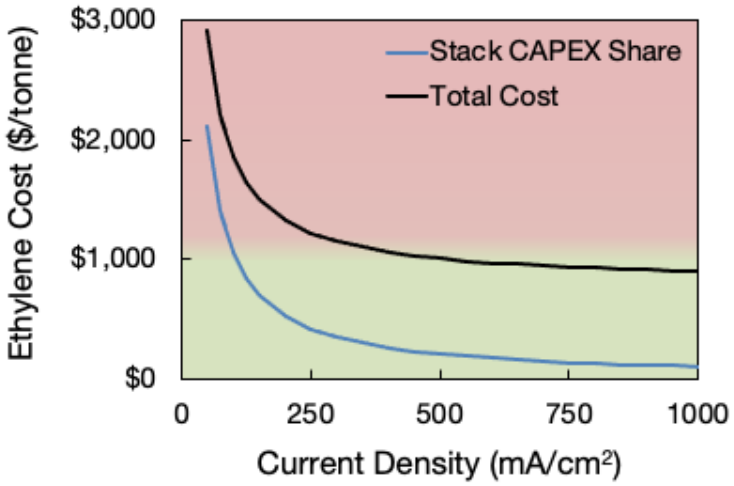

Figure 5: Electrolyzer stack CAPEX investment cost are levelized to a cost per tonne of ethylene and are shown as a function of current density. The total cost of ethylene production includes the stack CAPEX as well as all other capital and operational costs considered in [36].

As shown in Figure 5, the cost of ethylene production scales inversely with the current density of the reactor owing to the decreased stack area and material costs at higher current densities. The CAPEX of the electrolyzer stack is a driving cost component at low current densities, making operation at low current densities economically inviable when compared to conventional methods. Cost parity with conventional fossil fuel thermal methods is achieved at approximately 500mA/cm^2. Achieving such high current densities is critical to the eventual adoption of CO_2R technology. Furthermore, high activities must also be achieved under very stable conditions such that excessive electrode replacement is not required. The fundamental designs which have the potential to enable stable, high current density CO_2R operation are explored further herein.

3.4 Mass Transport Alleviation with Gas Diffusion Electrodes

The CO_2R mass transport bottleneck at the cathode is aptly demonstrated by observing the performance of H-cell systems, which were employed in early work by Hori et al. and see continued use for testing of novel catalysts. As shown in Figure 8a, the H-Cell configuration features a catalyst submerged in an electrolyte, with a significant distance l on the order of mm to cm between the CO_2 headspace and the catalyst. CO_2 must diffuse significant distances from the free surface where it dissolves to the catalyst surface, and thus the reaction rate is limited by

the CO_2 diffusion rate[38]. For this reason, H-Cell configurations are limited to just 10's of mA/cm^2, much lower than the 100's of mA/cm^2 necessary for commercial relevance.

This mass transport bottleneck can be alleviated by maintaining CO_2 in a gaseous phase in close proximity to the catalyst to reduce the distance which the CO_2 must diffuse to the order of micrometers or nanometers. This minimization is the fundamental motivation for the Gas Diffusion Electrode (GDE), an electrochemical architecture used for a variety of gas-phase electrochemical reactions such as Hydrogen fuel cells. GDE designs seek to maximize triple phase contact between the gas phase, electrolyte, and solid catalyst by using hydrophobic porous gas transport layers, known as Gas Diffusion Layers (GDL), which create a sharply defined interface between gas and electrolyte at which a catalyst is situated as shown in Figure 6.

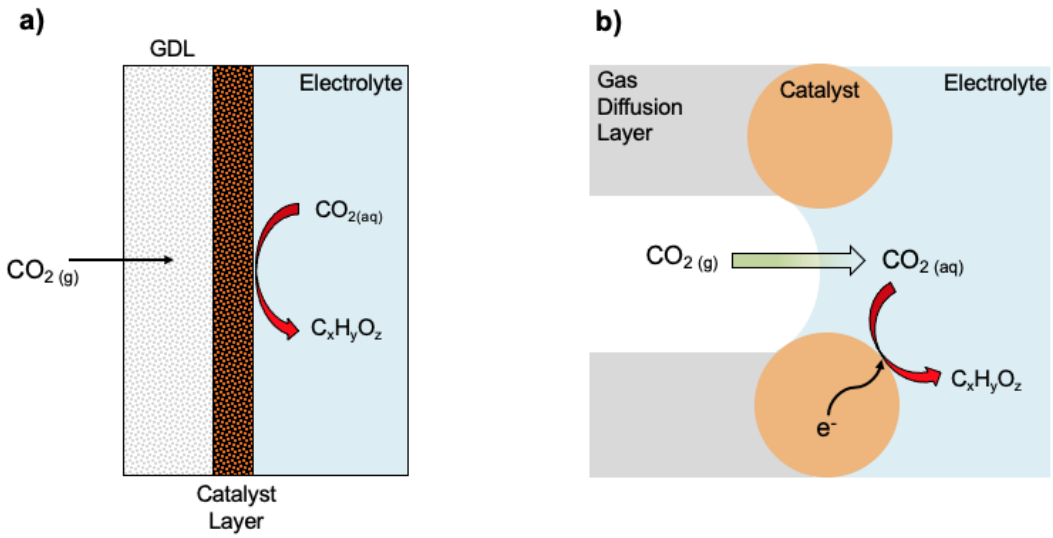

Figure 6: a) schematic representation of a GDE which is composed of the GDL and Catalyst Layer. The catalyst is in contact with the electrolyte, forming triple phase contact as shown in a microscopic representation in b). If the GDL is properly hydrophobic and resists wetting of the electrolyte, the CO_2 dissolves over the electrolyte-gas interfaces and must travel only a small distance on the order of micrometers before reacting at the catalyst.

The wetting state throughout the Gas Diffusion Electrode is crucial to the performance of the Gas Diffusion Electrode. If the catalyst is not wetted with electrolyte, the reaction cannot proceed as it does not have access to aqueous ions. On the other hand, wetting of the electrolyte

beyond the catalyst layer and into the porous GDL would eliminate the triple phase contact and result in increased CO_2 diffusion lengths. The reduced availability of CO_2 to the catalyst will enable parasitic competing reactions such as Hydrogen Evolution (HER) to occur, decreasing the overall selectivity of the reaction and current density towards CO_2R. This event, termed flooding, is critical to both the short-term performance and long-term stability of CO_2R systems and can be caused by variety of physicochemical factors[40]. Some mechanisms include imbalances in electrolyte and gas pressures, production of C_{2+} liquids which reduce the local electrolyte surface tension[41], salt formation within the gas diffusion layer[42], and voltage-induced degradation of hydrophobic coatings[39]. Though system design can alleviate some of these factors, others such as the formation of salt, liquid production, and voltage-induced degradation are exacerbated by increasing the current density of the reaction. Thus, the flooding resistance of a GDL can play a key limiting role of the current density possible without inducing a flooding event. The hydrophobic characteristics of the GDL which prevents flooding is thus of great interest moving forward.

In summary, the GDL plays four key roles: i) physically supports the catalyst, ii) allows for facile gaseous CO_2 transport to the triple phase contact line, iii) maintains stable triple-phase contact line of electrolyte/catalyst/CO_2 by preventing flooding, and iv) provides some electron conduction pathway to the catalyst layer. Requirements i) and ii) are simple physical constraints which constrain GDL designs to be porous and have ample gas permeability. The robust hydrophobicity and the conductivity requirements stand at odds in the GDL material design space. Typically, materials that are robustly hydrophobic are non-conductive polymers such as PTFE, while highly conductive materials tend to be hydrophilic, such as most metals. A GDL which is hydrophobic but lacking in conductivity may face significant ohmic losses and therefore be difficult to scale. A GDL which is conductive yet lacking in hydrophobicity will display poor flooding resistance and be limited to lower current densities and voltages. Three main classes of GDL design are present in the literature, which occupy distinctly different spaces in this design space. Metallic GDLs are highly conductive and have primarily found use for CO_2 reduction to CO[43,44], where the lack of liquid products coupled with the high catalytic selectivity of Ag and Zn catalysts abates the lack of hydrophobicity. Carbon paper is a composite GDL composed of a porous network of moderately conductive carbon fibers coated with a hydrophobic layer of PTFE. Carbon paper finds significant usage in fuel cells, where their hydrophobicity is adequate.

However, the PTFE coating on carbon paper does not provide adequately robust hydrophobicity to guarantee long term stable performance for CO2R, as it has been shown that the higher required voltages of -0.4V to -0.8V vs RHE cause the carbon paper to lose its hydrophobicity[39]. These systems typically fail due to flooding in 10's of hours of high-current density operation[45–48]. Finally, ePTFE membranes are a porous network of pure PTFE fibers with pore sizes in the 100's of nm to microns range. These membranes display highly robust hydrophobic behavior, and have been shown to maintain stable high-current density CO_2R to C_{2+} products for well over 100 hours[39,49–53] without failure. However, being composed of pure PTFE, these membranes are inherently electrically insulating, and electrons must be transported to the catalyst through the thin catalyst layer itself. Though efforts have been made to increase the conductivity of these designs, the conductance of these systems typically still remains lower than that of carbon paper[52].

This fundamental material tradeoff in the GDL design space plays a significant role in the efficiency and techno-economic feasibility of CO_2R at scale, as the attainable stable current density and the voltage of the cell are two key levers of process cost as previously shown. The absence of a GDL design with both the excellent hydrophobicity observed in ePTFE membranes and adequate conductivity presents an opportunity to design a next generation of GDLs which brings the field one step closer to techno-economic feasibility. The design of such a GDL lies within the future scope of this work, whether through material design or through system architecture design. In order to test and develop the next generation of GDLs, a test bench setup reactor was designed, and the choices factoring into that design are discussed next.

3.5 System Design

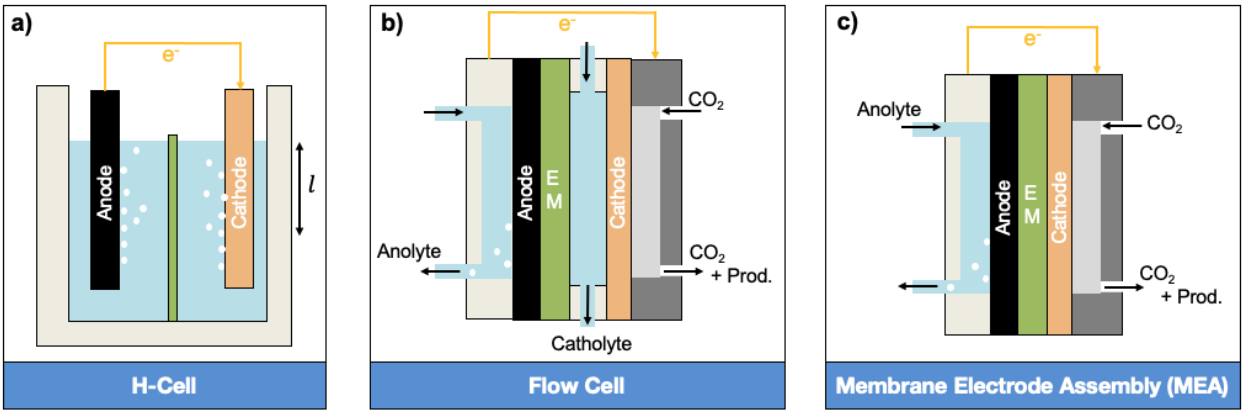

Figure 7: Schematics representing the a) H-Cell CO_2R configuration, b) Flow-Cell CO_2R configuration, c) MEA CO_2R configuration. The Flow Cell and MEA employ gas diffusion layers at the cathode, which minimizes the length *l* which aqueous CO_2 must travel. The long *l* on the order of mm to cm in the H-cell limits its practical CO_2 reduction current density.

Most GDEs are implemented in one of two CO_2R reactor systems, the flow cell and the membrane electrode assembly (MEA) as shown in Figure 8 b) and c)[54]. In the flow cell configuration, the cathode and anode have separate electrolyte streams (the catholyte and anolyte, respectively) that are separated by an ion exchange membrane (EM). Flow Cells offer a high degree of control over the pH and reaction conditions proximal to the catalyst via tuning of the catholyte composition. Highly alkaline conditions suppress the HER reaction, and thus it has been shown in flow cells that using solutions as concentrated at 10M KOH can increase selectivity and thus the limiting current density of CO_2R flow cell reactors to above 1A/cm2[53]. Though the alkalinity of the catholyte assists in maintaining a selective reaction, it also promotes the formation of carbonate at the CO_2/Electrolyte interface. This results in significant flux of carbonate over the anion exchange membrane, where carbonate is oxidized back into CO_2, reducing the single-pass conversion and incurring additional separation costs. Carbonate crossover ratios can be as high as 20, and incur significant energy and efficiency penalties for the regeneration of the electrolyte[36,43,55]. On the other hand, MEA configurations as shown in Figure 8c) have only an anolyte. The entire stack is compressed together such that the cathode catalyst contacts the ion exchange membrane where it receives the necessary ions to perform the reduction reaction. Due to the absence of a catholyte, the local reaction conditions in an MEA are

dictated by the production of ions from the reaction as well as transport over the membrane, and is thus more difficult to control. Without this degree of control, achievable current densities in MEA reactors are typically lower than that of flow cells, though neutral MEA systems due feature reduced carbonate crossover[36]. MEAs tend to maintain a higher degree of stability with less flooding concern compared to flow cells due to a limited presence of electrolyte and more controlled pressure conditions. The elimination of the catholyte in MEA systems also lends itself to the increased scalability of the MEA system over flowcells. Moreover, the use of thin ion membranes on the order of 50um allows for lower ohmic losses and decreased cell voltages in comparison to MEAs[52].

An MEA system design was selected to serve as a testbed for novel GDL designs on account of its expected increased stability, lower cell voltage, and lower carbonate crossover compared to a flow cell system.

3.6 Experimental Setup

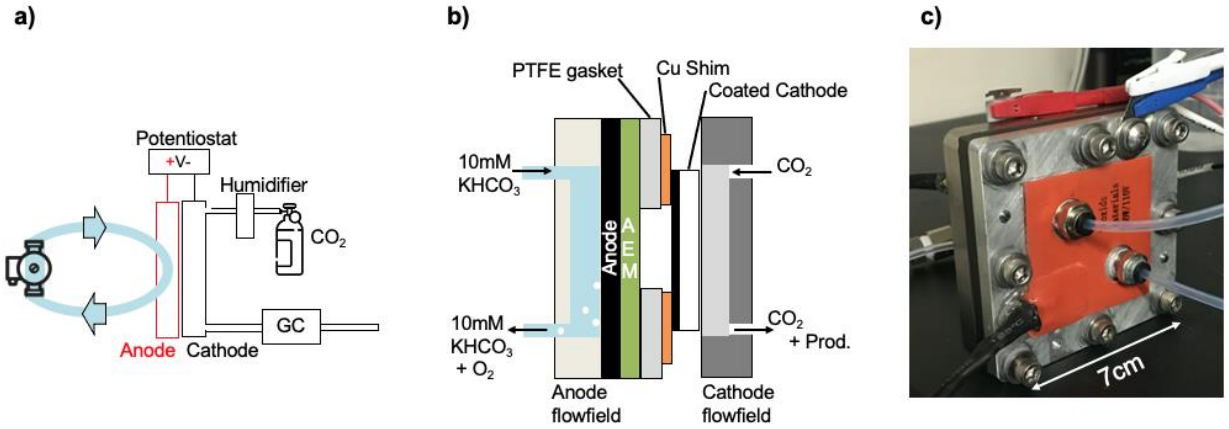

Figure 8: a) High-level diagram of the Electrochemical CO_2 reduction experimental setup. b) Cross-sectional view showing the internal MEA assembly stackup. c) Image of the assembled Electrochemical CO_2 reduction system, with the cathode flow field facing outwards.

As shown in Figure 9, an experimental setup was constructed to facilitate testing of the reactor and GDLs. A peristaltic pump (Easy-load 3, MasterFlex) was used to circulate the 10mM $KHCO_3$ anolyte from a 400mL reservoir through the anode flowfield at 60mL/min unless otherwise specified. The 10mM anolyte concentration was carefully selected, as concentrations

below 10mM result in decreased electrolyte conductivity and therefore increased ohmic losses, while the electrolyte concentrations above 10mM which were tested resulted in excessive salt formation. The salt formation eventually blocked the flow of CO_2 in the cathode flowfield as shown in Figure 10, causing decreased faradaic efficiencies and failure of the system. Pure CO_2 (99.995%, Airgas) was supplied to the cathode at a constant rate of 100SCCM for all experiments unless otherwise specified. PTFE 1/16" inner diameter tubing was used for all fluid flows. A humidifier was used to humidify the incoming CO_2 stream, though recent analyses suggest that the majority of reactant water in MEA systems is provided by transport across the membrane from the anolyte induced by electroosmotic drag[56]. The gaseous reaction products exiting the cell along with unreacted CO_2 are analyzed using an Agilent 7890A GC. An anion exchange membrane (AEM) physically separates the anode and cathode while maintaining ionic conductivity. Unless otherwise specified, the Dioxide Material Sustainion X-37 RT AEM is used. Figure 9c) shows the system as fully assembled. The leads of an SP-150 Potentiostat (BioLogic) are connected to the anode and cathode flowfields which also act as current collectors. When non-conductive PTFE GDLs were used, the cathode and cathode flowfield were electrically connected via a copper shim shown in Figure 9b) which made contact upon compression. The MEA assembly is compressed by eight #10-32 bolts, each torqued to between 4 and 6 N-m to yield appropriate compression of the anode and cathode GDL[43].

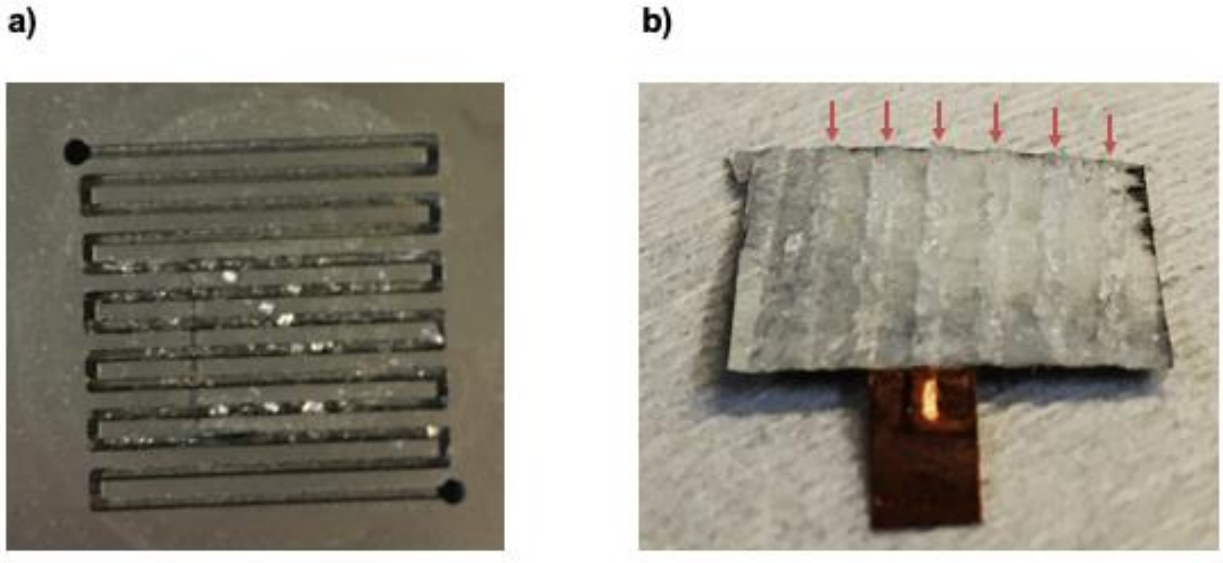

Figure 9: Salt formation in the cathode compartment after a 4 hour experiment with 0.1M KHCO3 anolyte. a) shows the residual salt in the flowfield, while b) shows the salt adhered to the back side of the PTFE GDL. The red arrows indicate where the GDL was in contact with the flow field channels, where the salt preferentially collects.

Both cathode and anode flowfields were machined with a serpentine flowpath geometry with slightly less than 50% open area and a track width of 1/32". The anode flowfield material is grade 2 titanium and was purchased directly from Dioxide Materials (DM). Titanium is the material of choice for the anode side as it is one of few metals which is stable under a highly oxidative environment[57]. Initial system iterations used stainless steel as the material for the cathode flowfield, but it was discovered that the stainless steel participates in undesired HER side reactions under certain conditions as shown in Figure 11. High-density graphite was thus used for the cathode flowfield for its relative inertness under reducing potentials while still having acceptable conductivity. The graphite flowfield was backed by an aluminum plate to increase structural integrity while improving conductivity and current collection.

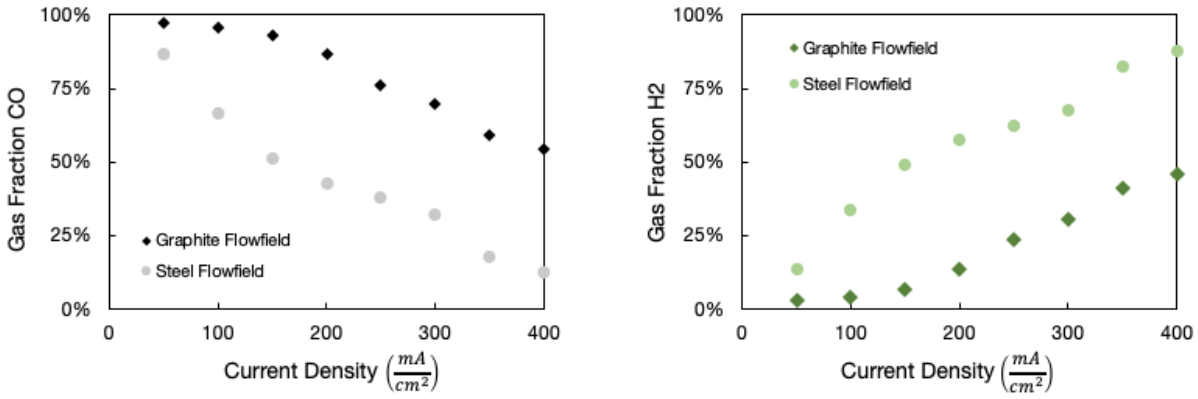

Figure 10: Gas fraction of CO and H_2 in the CO_2 reactor with graphite or stainless steel cathode flow field material. The cathode was silver filter paper in replication of Seger et al[43]. All parameters were held constant between the two experiments other than the flowfield material. The stainless steel flowfield shows a reduced CO gas fraction due to increased H2 generation, which is attributed to parasitic HER side reactions occurring on the SS flowfield.

3.7 Electrode Fabrication

3.7.1 Anode

Iridium Oxide is the predominantly used anode catalyst for OER, as it is broadly active and stable across acidic, neutral, and basic conditions[54]. For short-term tests, Iridium Oxide anodes with a loading of approximately 1.5mg/cm^2 on a carbon paper GDL were purchased directly from Dioxide Materials. However, the unstable oxidation of carbon into CO_2 under highly oxidative OER conditions renders these electrodes unusable for long-term or high-current density operation. This effect is explored experimentally in subsequent sections. In order to improve the long-term stability, we fabricated a second Iridium Oxide anode supported by a metallic Titanium mesh via a thermal deposition method[52,58]. The titanium mesh (Fuel Cell Store, 0.002" thickness) was etched in 6M HCL at 80-90C for 45 minutes to enhance connectivity and adherence of the IrOx. The mesh was then submerged into a solution containing 90mg $IrCl_3$, 30mL IPA, and 3mL concentrated HCl. The solution is boiled off at 100C, resulting in crystalline formation on the mesh. The mesh is then calcinated at 500C for 10 minutes to form Iridium Oxide.

3.7.2 Cathode

As we are more interested in GDLs and electrode architecutres than catalysis, a simple and reliable pure metallic Copper (Cu) catalyst was employed at the cathode. Two types of cathodes were fabricated, one using Sigracet 22B carbon paper GDL, and the other using an ePTFE membrane with 450nm pore size and 110um thickness (Sterlitech) as a GDL. These two cathodes are referred to as the "carbon-paper electrode" and the "ePTFE electrode". Magnetron RF Sputtering (AJA) was used to repeatably deposit copper onto the GDLs. A base vacuum of 5E-05 mtorr was reached before Cu deposition proceeded at a deposition pressure of 30mTorr and a rate of 0.833A/s which was verified via QCM. A deposition thickness of 250nm was targeted in light of previous catalyst thickness optimization studies[52]. The carbon-paper electrode and ePTFE electrode are shown in Figure 12.

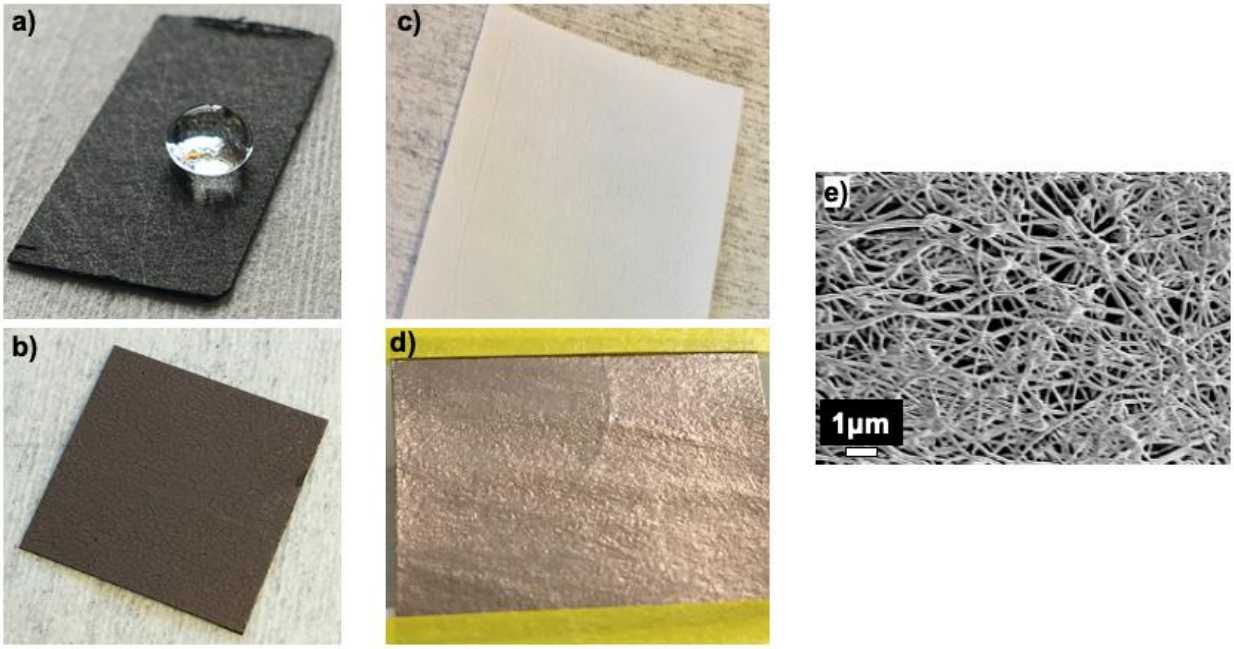

Figure 11: a) Carbon paper before 250 nm copper deposition and b) after deposition. The water droplet beaded up on the carbon paper in a) demonstrates the initial hydrophobicity of carbon-paper gas diffusion layers. c) Finely porous side of the ePTFE membrane before copper deposition and d) after 250nm of copper was deposited. E) SEM image of the copper-coated ePTFE network. There does not appear to be significant blockage of the pores.

3.8 Experimental Data

The performance of the carbon-paper electrode was characterized with regards to gaseous product selectivity and full cell voltage in chronopotentiometry mode, and is shown in Figure 13.

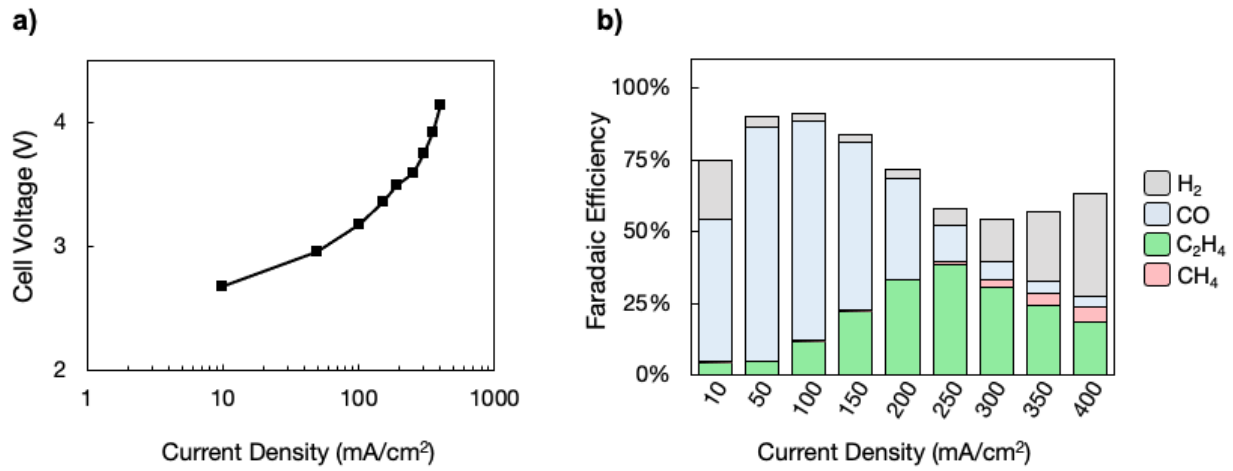

Figure 12: a) full cell voltage and b) faradaic efficiency of gaseous products in the MEA with a carbon paper IrOx anode and a 4.2cm^2 Cu carbon paper cathode. The faradaic efficiencies do not total to 100%, because only gaseous products were measured with the GC. The remaining faradaic efficiency is attributed to formation of liquid products. The minimum in total gas faradaic efficiency at 300mA/cm^2 is expected to align with the maximum production of liquids, particularly ethanol which has a similar overpotential required as ethylene.

At low current densities, the reactor produces primarily CO. As the current density and voltage increase, production of ethylene increases and reaches its peak at 39% faradaic efficiency at a current density of 250mA/cm^2 and a voltage of 3.6V. As the current density increases beyond 250mA/cm^2, the faradaic efficiency of ethylene begins to decrease due to increased hydrogen evolution. This is expected to occur at high overpotentials, as mass transport or other kinetic limitations constrain the CO_2R partial current. Methane production is also measured, reaching 6% FE at 400mA/cm^2.

In order to elucidate the flooding phenomenon in carbon-paper electrodes, a stability test was executed on the same Cu carbon-paper cathode with the carbon-paper IrOx anode, with the reaction held under chronopotentiometry at 150mA/cm^2.

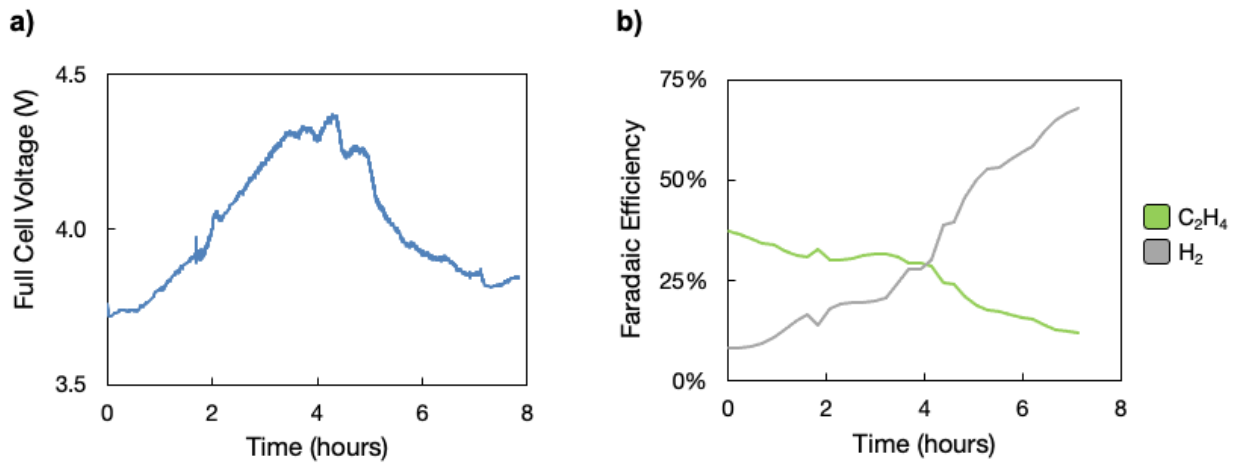

Figure 13: a) Full cell voltage and b) Faradaic Efficiency of the Cu carbon paper cathode and IrOx carbon paper anode over the course of an 8 hour uninterrupted test. The 400mL anolyte reservoir was not refreshed at any point during the test.

During the stability test, the FE attributed to Ethylene and Hydrogen are initially 37% and 8% respectively, matching closely the peak performance seen in Figure 13. The cell voltage in Figure 14a) climbs for the first 4 hours along with a minor decrease in the FE of ethylene. This initial increase in voltage is attributed to the oxidation of the anode support, and is discussed in the following section. After 4 hours, the full cell voltage begins to decrease, and is accompanied by a sharp decrease in ethylene FE and an increase in H_2 FE. This decrease in cell voltage is attributed to flooding of the electrolyte into the cathode which increases the available catalyst surface area. Once the cathode is submerged in electrolyte, the required diffusion distance of CO_2 to the catalyst is increased, which enables the competing HER. Significant moisture was discovered in the cathode compartment after disassembly, indicating that a flooding event did occur. After a 24 hour drying period, the carbon paper cathode did not regain its hydrophobicity, displaying a contact angle of less than 90 degrees. The observance of flooding for a carbon-paper cathode and the similar appearance of voltage and FE profiles as shown in literature validates the construction of the MEA testbed cell and elucidates the instability and flooding weakness of carbon-paper based cathodes[48,52].

To demonstrate the favorable flooding resistance of ePTFE-based GDLs, the carbon-paper cathode from the previous experiment was replaced with an ePTFE cathode. The same IrOx anode was used to isolate the effects of the cathode.

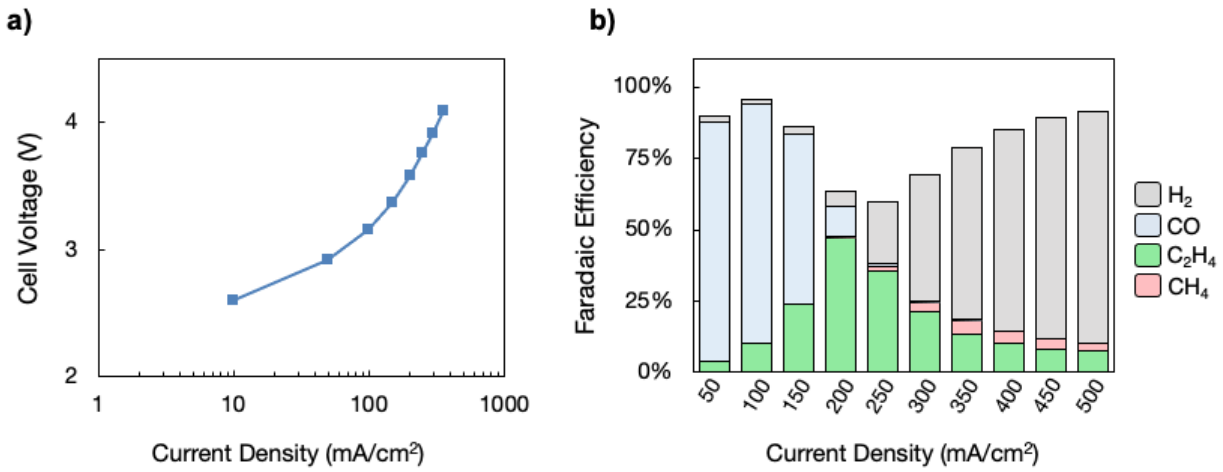

Figure 14: a) full cell voltage and b) faradaic efficiency of gaseous products in the constructed MEA with a carbon paper IrOx anode.

With regards to peak ethylene selectivity, the cathode with the ePTFE GDL outperforms the carbon-paper cathode. The ePTFE cathode reaches a peak Ethylene faradaic efficiency of 47% at 200mA/cm^2. At this current density, H_2 generation is held to only 5% FE and CO to 11% FE, indicating a very high C_{2+} conversion efficiency. Though liquid products were not measured for this experiment, assuming a total FE of 100% and that the remaining unaccounted products are all liquid C_{2+} products implies a C_{2+} FE of 84%. A subsequent stability test was undertaken at 200mA/cm^2 with results shown in Figure 16.

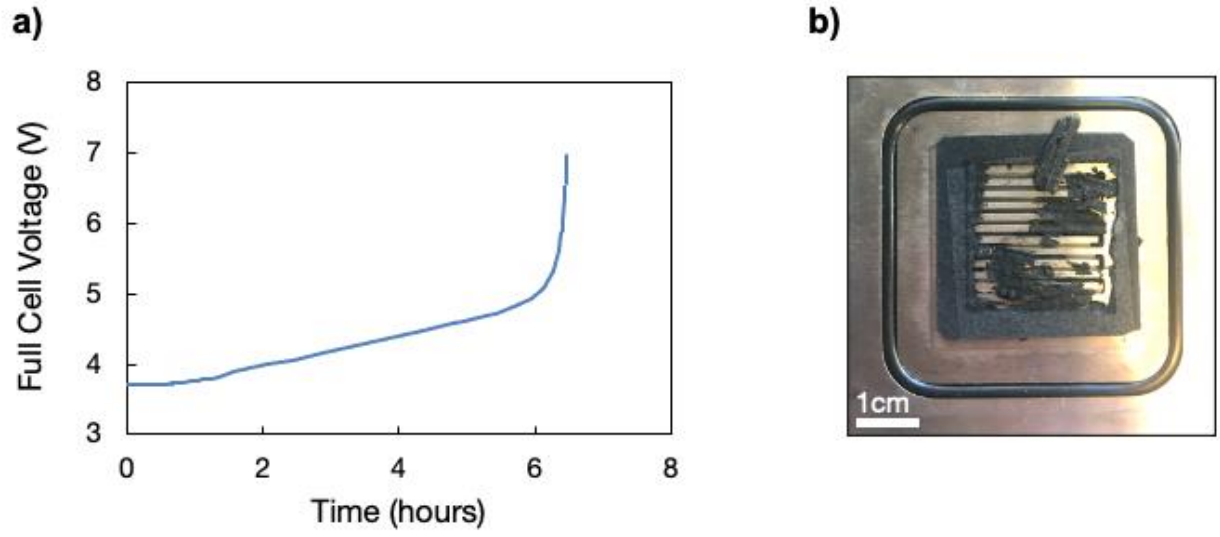

Figure 15: a) Cell voltage over the course of a 6 hour test using an ePTFE cathode and carbon-based IrOx anode. The test ended after 6 hours when the voltage exceeded the maximum allowable voltage of the potentiostat. b) Image of the carbon-based IrOx anode after the test. The active area of the anode disintegrated, compromising its mechanical and electrical integrity.

When subjected to a long-term stability test, the Cu ePTFE cathode / IrOx carbon-paper anode pair experienced significant instability. As shown in Figure 16, the full cell voltage increased steadily over the course of the test. This failure mode is distinct from the one observed for the carbon paper; a voltage drop characteristic of flooding was not observed. Moreover, the ePTFE GDL retained its super-hydrophobicity after it was removed from the cell and dried, further supporting the robust anti-flooding characteristics of the PTFE GDL. The instability is attributed to the anode: over the course of the test, the high oxidative potentials in combination with the presence of O_2 produced at the anode likely lead to oxidation of the Carbon within the anode carbon paper gas diffusion layer. This resulted in the disassociation of the IrOx anode's carbon support structure, reducing the electrical connectivity and increasing the full cell voltage. This phenomenon is believed to also occur in the cell using the carbon-based cathode. The initial increase in cell voltage in Figure 14 is attributed to this disintegration, before the cathode floods and decreases the cell voltage. This oxidative failure can be avoided by using stable metallic supports for the anode, such as Titanium. These anodes have been prepared and will be tested in future work.

3.9 Discussion

The design of a CO_2 conversion reactor was validated by reaching nearly 50% FE towards C_2H_4 at a current density of 200mA/cm^2. The observation of flooding in the case of the carbon-paper cathode confirmed the importance of Gas Diffusion Layer design for reaching the high-current density stability necessary for commercialization. ePTFE cathodes were shown to outperform carbon-paper based cathodes with respect to peak selectivity as well as flooding resistance and maintenance of hydrophobicity. While the low conductivity of ePTFE Gas Diffusion Layers was recognized, it was not experimentally addressed in this work. This falls within the scope of future work, which will entail designing GDLs whose performance exceeds those of carbon-paper based GDLs and ePTFE GDLs shown in the present work. The CO_2R

reactor designed and validated in this work will serve as the testbed for further development. These efforts to increase current density are a necessary development to reduce the overall cost of ethylene production, as current density is an important factor. Next steps include the development of a large-scale reactor and life cycle analyses to further guide technological development.

4 Conclusions

The maximum achievable current density was found to be a critical factor for the cost of both processes analyzed herein: pH electro-swing DOC and CO_2 Conversion. In order to establish economic viability and leverage these promising technologies at scale, developments which increase their current densities are needed. Though the CAPEX associated with Electrolyzer Stacks was the driving cost component for the DOC process, other risks items were identified, including infrastructure costs associated with CO_2-oceanwater separation and the consideration of costs associated with the intake of oceanwater. As for CO_2 conversion, the relationship between achievable current density and gas diffusion layer composition was explored. A reactor cell was designed, constructed, and validated to demonstrate the importance of gas diffusion layers and to establish a testbed for future electrode designs. The cell was validated to perform at levels comparable to that seen in the literature.

5 References

1. United Nations. Adoption of the Paris Agreement. (2015).
2. Net Zero by 2050 - A Roadmap for the Global Energy Sector. 224.
3. Tollefson, J. Sucking carbon dioxide from air is cheaper than scientists thought. *Nature* **558**, 173–173 (2018).
4. Keith, D. W., Holmes, G., St. Angelo, D. & Heidel, K. A Process for Capturing CO2 from the Atmosphere. *Joule* **2**, 1573–1594 (2018).
5. Carbon Negative Shot. *Energy.gov* https://www.energy.gov/fecm/carbon-negative-shot.
6. DeVries, T. The oceanic anthropogenic CO2 sink: Storage, air-sea fluxes, and transports over the industrial era. *Global Biogeochemical Cycles* **28**, 631–647 (2014).
7. Khatiwala, S. *et al.* Global ocean storage of anthropogenic carbon. *Biogeosciences* **10**, 2169–2191 (2013).
8. Andrew G. Dickson. Part 1: Seawater Carbonate Chemistry.
9. Eisaman, M. D. *et al.* CO2 extraction from seawater using bipolar membrane electrodialysis. *Energy Environ. Sci.* **5**, 7346–7352 (2012).
10. Eisaman, M. D. *et al.* Indirect ocean capture of atmospheric CO2: Part II. Understanding the cost of negative emissions. *International Journal of Greenhouse Gas Control* **70**, 254–261 (2018).
11. de Lannoy, C.-F. *et al.* Indirect ocean capture of atmospheric CO2: Part I. Prototype of a negative emissions technology. *International Journal of Greenhouse Gas Control* **70**, 243–253 (2018).
12. Digdaya, I. A. *et al.* A direct coupled electrochemical system for capture and conversion of CO2 from oceanwater. *Nat Commun* **11**, 4412 (2020).

13. Willauer, H. D., DiMascio, F., Hardy, D. R. & Williams, F. W. Development of an Electrolytic Cation Exchange Module for the Simultaneous Extraction of Carbon Dioxide and Hydrogen Gas from Natural Seawater. *Energy Fuels* **31**, 1723–1730 (2017).
14. Weiss, R. F. The solubility of nitrogen, oxygen and argon in water and seawater. *Deep Sea Research and Oceanographic Abstracts* **17**, 721–735 (1970).
15. PV PPA Prices | Electricity Markets and Policy Group. https://emp.lbl.gov/pv-ppa-prices.
16. Electric Power Monthly - U.S. Energy Information Administration (EIA). https://www.eia.gov/electricity/monthly/epm_table_grapher.php.
17. Green hydrogen cost reduction: Scaling up electrolysers to meet the 1.5C climate goal. 106.
18. *Analysis, synthesis, and design of chemical processes*. (Prentice Hall, 2009).
19. Is carbon capture too expensive? – Analysis. *IEA* https://www.iea.org/commentaries/is-carbon-capture-too-expensive.
20. Herzog, H. *et al.* Cost and economic potential. 24.
21. Herron, S., Zoelle, A. & Summers, W. M. *Cost of Capturing CO2 from Industrial Sources*. DOE/NETL-2013/1602, 1480985 http://www.osti.gov/servlets/purl/1480985/ (2014) doi:10.2172/1480985.
22. Crone, B. C., Garland, J. L., Sorial, G. A. & Vane, L. M. Significance of dissolved methane in effluents of anaerobically treated low strength wastewater and potential for recovery as an energy product: A review. *Water Res* **104**, 520–531 (2016).
23. The Future of Petrochemicals. *IEA* 132 (2018).
24. Zhu, Q. Developments on CO2-utilization technologies. *Clean Energy* **3**, 85–100 (2019).
25. Snoeckx, R. & Bogaerts, A. Plasma technology – a novel solution for CO2 conversion? *Chem. Soc. Rev.* **46**, 5805–5863 (2017).

26. Production of Bio-ethylene.
27. Wallace Tyner, Frazad Taheripour, Qianlai Zhuang, Dileep Birur, & Uris Baldos. Land Use Changes and Consequent CO2 Emissions due to US Corn Ethanol Production: A Comprehensive Analysis. (2010).
28. Production Costs of Alternative Transportation Fuels. (2013).
29. Koester, V. BASF – Working Intensely on Eco-Efficiency. *ChemViews* (2019) doi:10.1002/chemv.201900004.
30. What would it take for renewably powered electrosynthesis to displace petrochemical processes? https://www.science.org/doi/10.1126/science.aav3506.
31. Hori, Y., Kikuchi, K. & Suzuki, S. Production of co and ch4 in electrochemical reduction of co2 at metal electrodes in aqueous hydrogencarbonate solution. *Chem. Lett.* **14**, 1695–1698 (1985).
32. Hori, Y., Takahashi, R., Yoshinami, Y. & Murata, A. Electrochemical Reduction of CO at a Copper Electrode. *J. Phys. Chem. B* **101**, 7075–7081 (1997).
33. Hori, Y., Murata, A. & Takahashi, R. Formation of hydrocarbons in the electrochemical reduction of carbon dioxide at a copper electrode in aqueous solution. *J. Chem. Soc., Faraday Trans. 1* **85**, 2309–2326 (1989).
34. Kuhl, K. P., Cave, E. R., Abram, D. N. & Jaramillo, T. F. New insights into the electrochemical reduction of carbon dioxide on metallic copper surfaces. *Energy Environ. Sci.* **5**, 7050–7059 (2012).
35. Jouny, M., Luc, W. & Jiao, F. General Techno-Economic Analysis of CO2 Electrolysis Systems. *Ind. Eng. Chem. Res.* **57**, 2165–2177 (2018).

36. Sisler, J. *et al.* Ethylene Electrosynthesis: A Comparative Techno-economic Analysis of Alkaline vs Membrane Electrode Assembly vs CO2–CO–C2H4 Tandems. *ACS Energy Lett.* **6**, 997–1002 (2021).
37. Verma, S., Lu, S. & Kenis, P. J. A. Co-electrolysis of CO2 and glycerol as a pathway to carbon chemicals with improved technoeconomics due to low electricity consumption. *Nat Energy* **4**, 466–474 (2019).
38. Soto, Á. M., Lake, J. R. & Varanasi, K. K. Transient Effects Caused by Gas Depletion during Carbon Dioxide Electroreduction. *Langmuir* **38**, 1020–1033 (2022).
39. CO2 electroreduction to ethylene via hydroxide-mediated copper catalysis at an abrupt interface. https://www.science.org/doi/10.1126/science.aas9100.
40. Yang, K., Kas, R., Smith, W. A. & Burdyny, T. Role of the Carbon-Based Gas Diffusion Layer on Flooding in a Gas Diffusion Electrode Cell for Electrochemical CO2 Reduction. *ACS Energy Lett.* **6**, 33–40 (2021).
41. Leonard, M. E. *et al.* Editors' Choice—Flooded by Success: On the Role of Electrode Wettability in CO_2 Electrolyzers that Generate Liquid Products. *J. Electrochem. Soc.* **167**, 124521 (2020).
42. Xu, Y. *et al.* Self-Cleaning CO2 Reduction Systems: Unsteady Electrochemical Forcing Enables Stability. *ACS Energy Lett.* **6**, 809–815 (2021).
43. Larrazábal, G. O. *et al.* Analysis of Mass Flows and Membrane Cross-over in CO2 Reduction at High Current Densities in an MEA-Type Electrolyzer. *ACS Appl. Mater. Interfaces* **11**, 41281–41288 (2019).
44. Luo, W., Zhang, J., Li, M. & Züttel, A. Boosting CO Production in Electrocatalytic CO2 Reduction on Highly Porous Zn Catalysts. *ACS Catal.* **9**, 3783–3791 (2019).

45. Ma, W. *et al.* Electrocatalytic reduction of CO2 to ethylene and ethanol through hydrogen-assisted C–C coupling over fluorine-modified copper. *Nat Catal* **3**, 478–487 (2020).
46. Chen, X. *et al.* Electrochemical CO2-to-ethylene conversion on polyamine-incorporated Cu electrodes. *Nat Catal* **4**, 20–27 (2021).
47. Zhang, T. *et al.* Highly selective and productive reduction of carbon dioxide to multicarbon products via in situ CO management using segmented tandem electrodes. *Nat Catal* **5**, 202–211 (2022).
48. Larrazábal, G. O., Okatenko, V., Chorkendorff, I., Buonsanti, R. & Seger, B. Investigation of Ethylene and Propylene Production from CO2 Reduction over Copper Nanocubes in an MEA-Type Electrolyzer. *ACS Appl. Mater. Interfaces* **14**, 7779–7787 (2022).
49. Zhong, M. *et al.* Accelerated discovery of CO2 electrocatalysts using active machine learning. *Nature* **581**, 178–183 (2020).
50. Huang, J. E. *et al.* CO2 electrolysis to multicarbon products in strong acid. *Science* **372**, 1074–1078 (2021).
51. Li, F. *et al.* Molecular tuning of CO2-to-ethylene conversion. *Nature* **577**, 509–513 (2020).
52. Gabardo, C. M. *et al.* Continuous Carbon Dioxide Electroreduction to Concentrated Multi-carbon Products Using a Membrane Electrode Assembly. *Joule* **3**, 2777–2791 (2019).
53. CO2 electrolysis to multicarbon products at activities greater than 1 A cm−2. https://www.science.org/doi/10.1126/science.aay4217.
54. Vass, Á., Kormányos, A., Kószó, Z., Endrődi, B. & Janáky, C. Anode Catalysts in CO_2 Electrolysis: Challenges and Untapped Opportunities. *ACS Catal.* **12**, 1037–1051 (2022).
55. Rabinowitz, J. A. & Kanan, M. W. The future of low-temperature carbon dioxide electrolysis depends on solving one basic problem. *Nat Commun* **11**, 5231 (2020).

56. Liu, Z., Yang, H., Kutz, R. & Masel, R. CO 2 Electrolysis to CO and O 2 at High Selectivity, Stability and Efficiency Using Sustainion Membranes. *Journal of The Electrochemical Society* **165**, J3371–J3377 (2018).

57. Lettenmeier, P., Gago, A. S. & Friedrich, K. A. *Protective Coatings for Low-Cost Bipolar Plates and Current Collectors of Proton Exchange Membrane Electrolyzers for Large Scale Energy Storage from Renewables*. *New Technologies in Protective Coatings* (IntechOpen, 2017). doi:10.5772/intechopen.68528.

58. Luc, W., Rosen, J. & Jiao, F. An Ir-based anode for a practical CO2 electrolyzer. *Catalysis Today* **288**, 79–84 (2017).